

## Analysis of 3-D Frictional Contact Mechanics Problems by a Boundary Element Method<sup>\*</sup>

KEUM Bangyong, LIU Yijun (刘轶军)<sup>\*\*</sup>

Department of Mechanical Engineering, University of Cincinnati, P. O. Box 210072,  
Cincinnati, Ohio 45221-0072, USA

**Abstract:** The development of two boundary element algorithms for solving 3-D, frictional, and linear elastostatic contact problems is reported in this paper. The algorithms employ nonconforming discretizations for solving 3-D boundary element models, which provide much needed flexibility in the boundary element modeling for 3-D contact problems. These algorithms are implemented in a new 3-D boundary element code and verified using several examples. For the numerical examples studied, the results using the new boundary element algorithms match very well with the results using a commercial finite element code, and clearly demonstrate the feasibility of the new boundary element approach for 3-D contact analysis.

**Key words:** boundary element method; 3-D contact problems; nonconforming discretizations

### Introduction

The boundary element method (BEM) has a distinctive advantage in contact mechanics analysis over other numerical methods, because of its higher accuracy in stress analysis, easier meshing due to the reduction of dimensions of the model and smaller data files for pre- and post-processing. However, it seems that there has been no appropriate commercial BEM package or research code for the 3-D contact stress analysis, which can handle complicated 3-D models with some flexibilities in meshing. This prompted the research reported in this paper, which is aimed to develop a new BEM to solve 3-D contact mechanics problems with nonconforming discretizations, in which the two meshes on two contact patches do not need to match element by element. This can make the discretization and analysis of a contact problem by the BEM much easier for users.

Anderson and Allan-Persson's work<sup>[1]</sup> seems to be the first published paper on the BEM for 2-D contact problems. Some of the other papers on the BEM for 2-D contact problems can be found in Refs. [2-7]. The common characteristics in these BEM works are that they all adopt a direct technique with which contact constraints are directly imposed without using the penalty parameter or Lagrangian multiplier. Even though there were research results using different approaches like the flexibility matrix method<sup>[8]</sup>, or the gap element method<sup>[9]</sup> in the BEM, it seems that the direct constraint approach is more suitable for the BEM than for the finite element method (FEM) because tractions are direct output of the BEM solution. The Lagrangian multiplier or the penalty parameter which are the methods to impose contact constraints in the displacement-based FEM may not be beneficial for the BEM, though it may be possible to use those approaches in the BEM<sup>[10]</sup>. Like the FEM, the mathematical programming approach based on variational inequality form has also been used for the BEM<sup>[11]</sup>. Another interesting approach is to try to combine the advantages of the FEM and BEM. Landenberger and El-Zafrany's

---

Received: 2004-08-10

\* \* To whom correspondence should be addressed.

E-mail: yijun.liu@uc.edu; Tel: 1-513-556-4607;

Fax: 1-513-556-3390

work<sup>[9]</sup> adapted the BEM for bodies and the FEM for contact areas. On the contrary, Guyot et al.<sup>[12]</sup> used the FEM for bodies and the BEM for contact areas. Man's monograph<sup>[13]</sup> is a good starting point for applications of the BEM to contact problems even though it is for 2-D problems.

Dandekar and Conant's work<sup>[2]</sup> is valuable in understanding the BEM contact program for solving 2-D conformingly meshed problems. For nonconforming discretizations, Blazquez et al.<sup>[14]</sup> pioneered the initial work in 1992. Similar work can be found in Refs. [4,6]. Paris et al.<sup>[15]</sup> suggested using linear discontinuous elements for frictionless problems when using nonconforming discretizations.

The works mentioned above are all for 2-D problems and use the shape function approach in the contact search algorithm. In 1998, Blazquez et al. compared the approaches using shape functions and investigated the problems of this approach<sup>[16]</sup>. Blazquez et al.<sup>[17]</sup> proposed a new approach to remedy the problem arising from using the shape function approach. In 1992, Chen and Chen<sup>[18]</sup> proposed the transformation matrix method for 2-D contact problems with friction. They claimed that the method was highly efficient. In 1998, Martin and Aliabadi<sup>[19]</sup> published a new approach for nonconforming mesh for 2-D contact problems. They utilized the fact that inside the element which is a smooth curve, an additional equation for the traction can be obtained by a singularity removal technique. In 1999, Iban et al.<sup>[20]</sup> proposed a new approach. They developed a variable shape function, in which the center node of the quadratic line element can move. The moving center node matches the node of the other body. By this method, the node-on-point situation became the node-to-node situation.

For 3-D problems, Garrido et al.<sup>[21]</sup> did the first work for the frictional contact analysis in 1994. Their formulation was based on an incremental form and used a triangular constant element. Yamazaki et al.<sup>[10]</sup> published in 1994 a penalty parameter-based method using 8-node quadratic elements. Segond and Tafreshi<sup>[7]</sup> used linear triangular elements for the frictionless problem in 1998. The advantage of Segond's work is that there exists analytical integration for the linear triangular element. In 1998, Ghaderi-Panah and Fenner<sup>[22]</sup> published the work on the quadratic element method for the frictionless problem. Their formulation

was based on the relatively simple contact condition of the frictionless problem and used the 9-node Lagrangian element to model the contact region. Leahy and Becker's work<sup>[23]</sup> was based on localized contact variables. They used 8-node quadratic elements and aimed at frictional problems.

All the above-mentioned work for 3-D elastostatic contact problems employed conforming meshes in the BEM. There has been no reported work on the development of 3-D BEM with nonconforming discretizations, according to the best knowledge of the authors.

In this paper, new BEM algorithms employing nonconforming discretizations for solving 3-D frictional contact problems are presented, which will facilitate easier BEM modeling of 3-D contact analysis. These algorithms are implemented in a new 3-D BEM code and verified using several numerical examples. These numerical studies are carried out using both the developed BEM code and a commercial FEM code. The results using the new BEM algorithms with nonconforming discretizations match well with the FEM results, and clearly demonstrate the feasibility and flexibility of the new BEM approach for 3-D contact analysis.

## 1 Basic Equations and Approaches for Contact Analysis

### 1.1 Basic equations

The main governing equations for contact mechanics analysis in static cases are:

$$\sigma_{ij} + b_i = 0 \quad (1)$$

where  $\sigma_{ij}$  is the stress and  $b_i$  the body force. In addition to Eq. (1), stress-strain and strain-displacement equations are necessary as in other elasticity problems. However, constraint equations from contact phenomena should be observed uniquely for contact problems. These constraint conditions are:

$$g(X) = 0, \quad X \in \Gamma_c \quad (2)$$

$$\mathbf{t} \cdot \mathbf{n} = t_n \leq 0 \quad (3)$$

$$|\mathbf{t} - t_n \mathbf{n}| = \mu t_n \quad (4)$$

in which  $g(X)$  is the distance between the two bodies for a point set  $X$ ,  $\Gamma_c$  the boundary where contact occurs,  $\mathbf{t}$  the traction vector, and  $\mathbf{n}$  the outward normal vector.

Equation (2) means that there should be no penetration between the two bodies engaged in contact. Equation

(3) means that normal traction should be of the pressure type, i.e., in a direction opposite to the normal vector of the surface. Equation (4) represents the relationship between the tangential traction and the normal traction. The coefficient  $\mu$  is the friction constant for the Coulomb friction model.

Solving contact problems requires calculation of the following variables: 1) contact area; 2) magnitude and distribution of normal and tangential tractions; 3) contact state (stick and slip); and 4) global displacement and stress fields. The characteristics of the stress solution for a point exhibit abrupt changes depending on whether the point is in the contacted region or non-contacted region and whether it is in the stick region or the slip region. This fact makes the contact problem one of the most difficult nonlinear mechanics problems.

Hertz's work was the first analytical approach to find the solution of contact problems. He simplified the problem based on five assumptions, with which he presented solutions for some contact problems with simple geometries<sup>[24]</sup>. When any of the Hertz's assumptions is not satisfied, the problem is called non-Hertzian. Though many efforts of extending the Hertz's approach have been made<sup>[25]</sup> in the past, analytical solutions are still limited to simple cases. The work of Johnson<sup>[25]</sup> and Gladwell<sup>[26]</sup> can be referred to for more details in this regard. Numerical methods, such as the finite element and boundary element methods, are therefore the only practical methods for solving large-scale contact problems involving arbitrary geometric and load conditions.

## 1.2 Conforming and nonconforming contact problems

Conforming contact problems means that apparent area of contact is known *a priori*. A good example of conforming contact problems is the flat punch problem. For a nonconforming contact problem, the apparent area of contact is not known *a priori*. Initially, the contact of a nonconforming problem is a line or point contact. The cylinder on cylinder problem is a case of nonconforming contact problems.

## 1.3 Conforming and nonconforming discretizations

To use numerical methods, such as the FEM and BEM, the geometric model must be discretized as elements

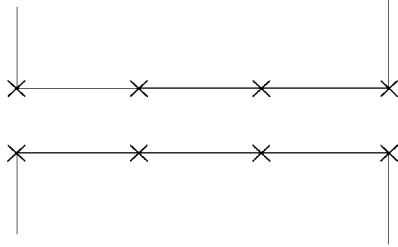
and corresponding nodes. Conforming discretization uses the same number of elements for each contacting patch on the two related bodies. The size and pattern of the elements on the two matching patches should also be close to each other as much as possible to reduce the error. Conforming mesh is required when the gap element approach or node-to-node approach in contact analysis is used. Therefore, a conforming mesh with gap elements or node pairs is more appropriate for solving the conforming contact problem. For the nonconforming contact problem, conforming mesh with gap elements or node pairs can still be used, but it is inherently limited to linear elastic problems because the size of element length cannot be matched exactly for large deformation cases.

Nonconforming discretization uses a different number of elements on the two contact patches and thus is easier for the discretization. The nonconforming mesh requires a different algorithm to solve contact problems. The approaches are usually based on node-to-surface, surface-to-surface, or node-to-point algorithms. Each of these approaches has many variations and these approaches are developed later historically than the node-to-node or gap element approaches. In general, node-to-point, node-on-point, node-to-surface, and node-on-surface can be regarded as synonyms in a broad sense though their meanings may be different in different articles. In this paper, these terms will be used to refer to the same meaning—nonconforming discretization.

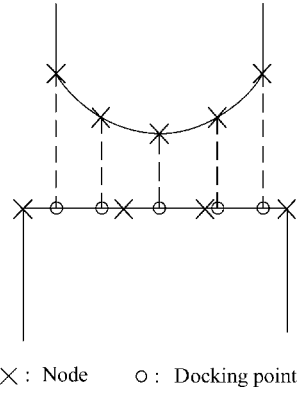
Usually, a conforming contact problem is easier to discretize with a conforming mesh and a nonconforming contact problem is easier to discretize with a nonconforming mesh. Figure 1 shows examples of conforming and nonconforming meshes. For a nonconforming discretization, a docking point is defined as shown in Fig.1b. A node and its corresponding docking point are called a control pair.

The reasons for using nonconforming discretizations include: 1) For problems that result in large deformation or large displacement, even an initially conforming discretized mesh can become a nonconforming mesh as the load is applied. 2) For some problems, the geometry is so complex that it is difficult or impossible to discretize using a conforming mesh. 3) The analyst may want a quick and easy mesh because the accuracy of the result is relatively less important or the result with a nonconforming mesh is believed to be

sufficiently accurate compared to the result with a conforming mesh. In short, the ability to solve a contact problem with nonconforming mesh is the first step to solve more advanced or realistic problems.



(a) Conforming geometry with conforming discretization



× : Node    o : Docking point

(b) Nonconforming geometry with nonconforming discretization

**Fig. 1 Examples of conforming and nonconforming contact and discretizations**

## 2 BEM Formulation for Contact Analysis

The boundary integral equation (BIE) for 3-D linear and elastostatic problems can be written as

$$C_{ij}u_j(P) + \int_{\Gamma} T_{ij}(P, Q)u_j(Q)dS(Q) = \int_{\Gamma} U_{ij}(P, Q)t_j(Q)dS(Q) \quad (5)$$

where  $T_{ij}$  is the traction kernel (from the fundamental solution),  $U_{ij}$  the displacement kernel,  $C_{ij}$  the coefficients which vary depending on the smoothness of the boundary  $\Gamma$ , and  $P$  and  $Q$  are the source point and field point, respectively. Derivation of Eq. (5) and related theory can be found in many BEM textbooks (see, e.g., Refs. [27-29]).

To apply the BEM to solve the BIE (Eq. (5)), it is necessary that the boundary variables be interpolated on all the boundary elements used to discretize the boundary  $\Gamma$ . For example, the interpolated variables on

a typical element can be expressed as:

$$x_i = \sum_{c=1}^{n_e} N_c(\xi, \eta)(X_i)_c \quad (6)$$

$$u_i = \sum_{c=1}^{n_e} N_c(\xi, \eta)(U_i)_c \quad (7)$$

$$t_i = \sum_{c=1}^{n_e} N_c(\xi, \eta)(T_i)_c \quad (8)$$

where  $X_i$ ,  $U_i$ , and  $T_i$  are nodal values of the Cartesian coordinates  $x_i$ , displacement, and traction, respectively;  $N_c$  shape functions with  $(\xi, \eta)$  being the natural coordinates and  $n_e$  the number of nodes on the element. For convenience, the shape functions for surface 3-, 4-, 8-, and 9-node elements used in this paper are listed in the Appendix.

With the chosen interpolation, the discretized BIE (Eq. (5)) for a source point  $P_k$  at a boundary node can be written as

$$\begin{bmatrix} C_{xx}(P_k) & C_{xy}(P_k) & C_{xz}(P_k) \\ C_{yx}(P_k) & C_{yy}(P_k) & C_{yz}(P_k) \\ C_{zx}(P_k) & C_{zy}(P_k) & C_{zz}(P_k) \end{bmatrix} \begin{Bmatrix} (U_x)_k \\ (U_y)_k \\ (U_z)_k \end{Bmatrix} + \sum_{m=1}^M \sum_{c=1}^{n_e} \begin{bmatrix} H_{xx} & H_{xy} & H_{xz} \\ H_{yx} & H_{yy} & H_{yz} \\ H_{zx} & H_{zy} & H_{zz} \end{bmatrix}_m \begin{Bmatrix} (U_x)_{c,m} \\ (U_y)_{c,m} \\ (U_z)_{c,m} \end{Bmatrix} = \sum_{m=1}^M \sum_{c=1}^{n_e} \begin{bmatrix} G_{xx} & G_{xy} & G_{xz} \\ G_{yx} & G_{yy} & G_{yz} \\ G_{zx} & G_{zy} & G_{zz} \end{bmatrix}_m \begin{Bmatrix} (T_x)_{c,m} \\ (T_y)_{c,m} \\ (T_z)_{c,m} \end{Bmatrix} \quad (9)$$

in which  $M$  is the total number of elements, the  $\mathbf{H}$  submatrices are obtained from integrating the  $T_{ij}$  kernel, while the  $\mathbf{G}$  submatrices from the  $U_{ij}$  kernel, on the elements. The final form of the discretized BIE can be represented as a linear algebraic system as follows by assembling the equations at all the nodes and imposing the boundary conditions (see, e.g., Ref. [30]):

$$\mathbf{A}\mathbf{d} = \mathbf{f} \quad (10)$$

where  $\mathbf{A}$  is the coefficient matrix,  $\mathbf{d}$  the vector of unknown boundary variables, and  $\mathbf{f}$  the known right-hand side vector. Because the values of the given boundary conditions at many nodes are zero, integrations for the element having zero boundary conditions can be skipped. This can save some CPU time in the matrix formation.

Because multiple bodies are involved in contact mechanics, the main issue in the contact BEM analysis is that the formation of the system matrix for each body is needed first. Then, the system matrix of each body will be combined to form the system matrix for the whole contact system. Incremental form combined with iterations is necessary to solve nonlinear contact problems using linearized system matrices.

First, a new total external force is represented as

$$F_{j,m} = F_{j,m-1} + \Delta F_{j,m} \quad (11)$$

where  $\Delta F_{j,m}$  is the increment of the load at step  $m$ , with  $m = 1, 2, \dots$ , total number of load steps. The traction and displacement corresponding to the increment of load (11) are:

$$\begin{aligned} u_{j,m} &= u_{j,m-1} + \Delta u_{j,m}, \\ t_{j,m} &= t_{j,m-1} + \Delta t_{j,m} \end{aligned} \quad (12)$$

When Eqs. (12) are inserted into Eq. (1), we can obtain the following incremental form of the BIE:

$$\begin{aligned} C_{ij} \Delta u_{j,m} + \int_{\Gamma} T_{ij}(P, Q) \Delta u_{j,m} dS(Q) = \\ \int_{\Gamma} U_{ij}(P, Q) \Delta t_{j,m} dS(Q) \end{aligned} \quad (13)$$

In Eq. (13), the boundary for each body is divided as follows (Fig. 2):

$$\begin{aligned} \Gamma &= \Gamma_t + \Gamma_u + \Gamma_{pc}, \\ \Gamma_{pc} &= \Gamma_{nc} + \Gamma_{rc}, \\ \Gamma_{rc} &= \Gamma_{st} + \Gamma_{sl} \end{aligned} \quad (14)$$

First representation of Eqs. (14) means that the boundary for each body ( $\Gamma$ ) is divided into three types: the boundary where traction is given ( $\Gamma_t$ ), the boundary where displacement is given ( $\Gamma_u$ ), and the assigned boundary where contact is possible to occur ( $\Gamma_{pc}$ ). The second representation of Eqs. (14) means that the contact occurs at some part of the assigned contact area. This fact requires that the first iteration loop at each load step should be used to distinguish the possible contact area ( $\Gamma_{pc}$ ) as the region where contact occurs ( $\Gamma_{rc}$ ) and the region where contact does not occur ( $\Gamma_{nc}$ ). The last representation of Eqs. (14) means that there are two regions inside the contact area. The second iteration loop at each load step is therefore used to divide the contact area ( $\Gamma_{rc}$ ) into two different regions—stick region ( $\Gamma_{st}$ ) and slip region ( $\Gamma_{sl}$ ). Note that for the possible contact region ( $\Gamma_{pc}$ ), both displacement and traction are unknown variables.

Therefore, the system matrix is underdetermined at the current step.

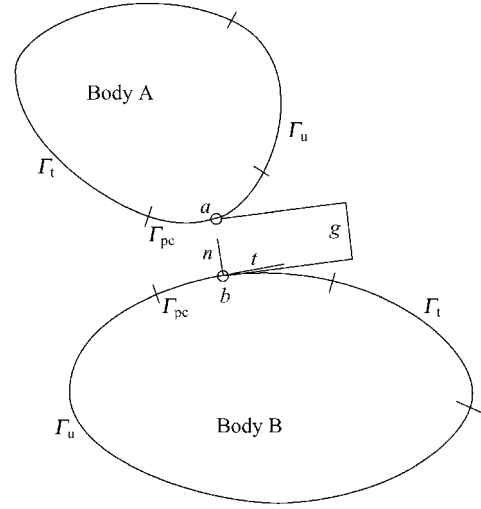


Fig. 2 Schematic diagram — Point  $a$  or  $b$  is either a node or a point on body A or body B

### 3 Contact Modes and Algorithms

For each iteration, the contact status is checked to see if the compatibility or equilibrium is violated or not. After the contact mode is determined, the corresponding contact constraint equations are added to the underdetermined systems in the BEM. This iteration continues until the compatibility and equilibrium are satisfied. Then, the load step is increased and the procedure is repeated for the next load step.

As anticipated, the more the nodes are in the possible contact region, the slower the calculation because more iterations are needed. However, in order to obtain reasonable results, a minimum number of elements should be employed in the contact region.

In the stick mode, the constraint equations are:

$$\begin{aligned} \Delta(t_a^{t1})_m - \Delta(t_b^{t1})_m &= -[(t_a^{t1})_{m-1} - (t_b^{t1})_{m-1}], \\ \Delta(t_a^{t2})_m - \Delta(t_b^{t2})_m &= -[(t_a^{t2})_{m-1} - (t_b^{t2})_{m-1}], \\ \Delta(t_a^n)_m - \Delta(t_b^n)_m &= -[(t_a^n)_{m-1} - (t_b^n)_{m-1}], \\ \Delta(u_a^{t1})_m + \Delta(u_b^{t1})_m &= 0, \\ \Delta(u_a^{t2})_m + \Delta(u_b^{t2})_m &= 0, \\ \Delta(u_a^n)_m + \Delta(u_b^n)_m &= g_0 - [(u_a^n)_{m-1} + (u_b^n)_{m-1}] \equiv g_{0,m} \end{aligned} \quad (15)$$

where  $g$  is the distance between points  $a$  and  $b$  (Fig. 2). The super scripts  $n$ ,  $t1$ , and  $t2$  mean the normal direction and two tangential directions, respectively.

In the slip mode, the constraint equations are:

$$\begin{aligned}
 \Delta(t_a^{t1})_m - \Delta(t_b^{t1})_m &= -\left[(t_a^{t1})_{m-1} - (t_b^{t1})_{m-1}\right], \\
 \Delta(t_a^{t2})_m - \Delta(t_b^{t2})_m &= -\left[(t_a^{t2})_{m-1} - (t_b^{t2})_{m-1}\right], \\
 \Delta(t_a^n)_m - \Delta(t_b^n)_m &= -\left[(t_a^n)_{m-1} - (t_b^n)_{m-1}\right], \\
 \Delta(t_a^{t1})_m \pm \mu \Delta(t_a^n)_m &= -\left[(t_a^{t1})_{m-1} \pm \mu (t_a^n)_{m-1}\right], \\
 \Delta(t_a^{t2})_m \pm \mu \Delta(t_a^n)_m &= -\left[(t_a^{t2})_{m-1} \pm \mu (t_a^n)_{m-1}\right], \\
 \Delta(u_a^n)_m + \Delta(u_b^n)_m &= g_0 - \left[(u_a^n)_{m-1} + (u_b^n)_{m-1}\right] \equiv g_{0,m} \quad (16)
 \end{aligned}$$

And in the separation mode, the constraint equations are:

$$\begin{aligned}
 \Delta(t_a^{t1})_m - \Delta(t_b^{t1})_m &= -\left[(t_a^{t1})_{m-1} - (t_b^{t1})_{m-1}\right], \\
 \Delta(t_a^{t2})_m - \Delta(t_b^{t2})_m &= -\left[(t_a^{t2})_{m-1} - (t_b^{t2})_{m-1}\right], \\
 \Delta(t_a^n)_m - \Delta(t_b^n)_m &= -\left[(t_a^n)_{m-1} - (t_b^n)_{m-1}\right], \\
 \Delta(t_a^{t1})_m &= -\left[(t_a^{t1})_{m-1}\right], \\
 \Delta(t_a^{t2})_m &= -\left[(t_a^{t2})_{m-1}\right], \\
 \Delta(t_a^n)_m &= -\left[(t_a^n)_{m-1}\right] \quad (17)
 \end{aligned}$$

The equations used to check and change the contact status from separate to contact and vice versa are:

$$\begin{aligned}
 (\Delta u_a^n + \Delta u_b^n)_m &\geq g_{0,m-1}, \\
 t_{m-1}^n + \Delta t_m^n &< 0 \quad (18)
 \end{aligned}$$

The equations used to check and change the contact status from slip to stick and vice versa are:

$$\begin{aligned}
 |t_{m-1}^t + \Delta t_m^t| &\geq \left| \mu (t_{m-1}^n + \Delta t_m^n) \right|, \\
 (t_{m-1}^n + \Delta t_m^n)_b &(\Delta u_a^t + \Delta u_b^n)_m \leq 0 \quad (19)
 \end{aligned}$$

## 4 Methods to Solve Contact Problem with Nonconforming Meshes

For the node-to-node approach,  $a$  and  $b$  in Fig. 2 represent nodal values in each body. However, for the node-to-point approach, one of the variables, for example  $b$ , represents a point which is inside an element in the contact area. This situation occurs when nonconforming meshes are employed and algorithms to represent the variables at the point  $b$  are needed. In this section, explanations about the differences in some node-to-point algorithms will be given in order to understand the advantages and disadvantages of each algorithm. It must be pointed out that none of these

algorithms are implemented for 3-D BEM in the literature.

### 4.1 Shape-function approach

This approach is the simplest one. The displacement and traction inside an element at point  $b$  can be represented as:

$$\begin{aligned}
 u_{i,b} &= \sum_{c=1}^{n_e} N_c(\xi_b, \eta_b)(U_i)_c, \\
 t_{i,b} &= \sum_{c=1}^{n_e} N_c(\xi_b, \eta_b)(T_i)_c \quad (20)
 \end{aligned}$$

One advantage of this approach is that it is simple conceptually and easy to implement. This algorithm is also applicable to 3-D problems. When applying this approach to 3-D problems with quadratic element, 9-node Lagrange element may be better because it has complete second-order shape functions.

### 4.2 Variable shape-function approach

In this approach, the shape functions for a 3-node line element with a moving middle node for 2-D problems are:

$$\begin{aligned}
 N_1(\xi) &= \frac{(\xi-1)(\xi-\kappa)}{2(1+\kappa)}, \\
 N_2(\xi) &= \frac{(\xi-1)(\xi+1)}{(-1+\kappa)(1+\kappa)}, \\
 N_3(\xi) &= \frac{(\xi+1)(\xi-\kappa)}{2(1-\kappa)} \quad (21)
 \end{aligned}$$

where  $\kappa$  is the natural coordinate of the center node. The advantage of this approach is its accuracy due to the fact that the node-to-point problem is changed to a node-to-node problem. However, it is complicated to implement (the center node should be checked and moved as the node pair is in stick or slip mode) and cannot be easily extended to 3-D problems.

### 4.3 BIE approach

This idea is based on the fact that a boundary element is always a smooth curve (2-D) or smooth surface (3-D). Thus, the displacement and traction at any point  $b$  on an element can be evaluated using the displacement BIE (Eq. (5)) and traction BIE (derivative of Eq. (5)), respectively.

The advantages of this approach are that the displacement and traction calculated from the BIEs are

more accurate theoretically. The system is also more stable compared to the shape-function approach because the equations from this approach are global contrary to the equations from shape functions which are local. The disadvantages are that, for each node in the contact region, numerical integrations need to be performed, such that the CPU time to build the system matrix for each iteration is increased compared to the shape-function approach. Also, the traction BIE has hypersingular integrals and special treatments need to be employed to either remove or compute the hypersingular integrals.

## 5 Two BEM Algorithms for 3-D Contact Analysis

In this paper, two new algorithms that adapt the BIE approach to 3-D contact problems with nonconforming meshes are developed, because of advantages that the BIE approach offers. The main idea and difficulties in extending the 2-D concept to 3-D problems are described in this section. The new algorithms will provide the contact constraint equations that can be added to the underdetermined linear system of equations.

### 5.1 The first method

The main idea of the first new algorithm is to extend the BIE approach to 3-D problems. The concept of this approach is depicted in Fig. 3. Even though it seems simple to extend the 2-D idea to 3-D, there are many technical difficulties to overcome. Some of the difficulties are from the BEM itself (singularities of kernels, especially in the traction kernel) and some of them are from the complications of programming for contact problems. These may be part of the reasons why there has been no published work regarding 3-D BEM for contact problems with nonconforming discretizations.

The first difficulty is the singularities of the integrand of BIEs. The singularity occurs for each docking point when the integration on the element where the docking point locates is performed. In this approach, the traction BIE is not employed for evaluating the traction at the docking point, since the cost of computing the system matrix will become too high and the difficulties will exist in dealing with the singular integrals. Thus, for the surface of one of the bodies in contact (let it be called slave surface), the shape function

approach is used to evaluate the traction at point  $b$  instead in order to form the system matrix.

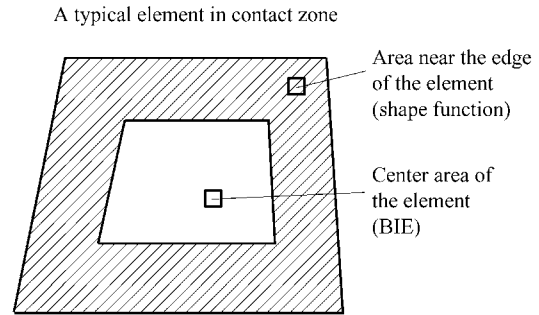


Fig. 3 Concept of the first algorithm: if a docking point is inside the hatched area of an element in the contact zone, the shape function approach is used. The BIE approach is used otherwise. (□) Indicates a docking point.

However, the displacement BIE is employed to evaluate the displacement at the docking point. Transformation of the variable method is used to deal with the singular kernels in the displacement BIE. For example, the variables on an element will be changed using:

$$\begin{aligned}\xi &= \sum_{c=1}^3 \bar{N}_c(\bar{\xi}, \bar{\eta}) \xi_c, \\ \eta &= \sum_{c=1}^3 \bar{N}_c(\bar{\xi}, \bar{\eta}) \eta_c\end{aligned}\quad (22)$$

where

$$\begin{aligned}\bar{N}_1 &= \frac{1}{4}(1 + \bar{\xi})(1 - \bar{\eta}), \\ \bar{N}_2 &= \frac{1}{4}(1 + \bar{\xi})(1 + \bar{\eta}), \\ \bar{N}_3 &= \frac{1}{2}(1 - \bar{\xi})\end{aligned}\quad (23)$$

which are linear interpolations. And

$$\bar{J} = \frac{\partial \xi}{\partial \bar{\xi}} \frac{\partial \eta}{\partial \bar{\eta}} - \frac{\partial \eta}{\partial \bar{\xi}} \frac{\partial \xi}{\partial \bar{\eta}}\quad (24)$$

Since the new Jacobian in Eq. (24) is of order  $O(r)$ , one order of the singularity is removed from the new integrand. Therefore, the displacement kernel becomes regular and the traction kernel becomes weakly singular for the displacement BIE. Some work about integrating strongly singular kernels in 3-D BEM was published earlier<sup>[31-33]</sup>. The method used here for dealing with the strongly-singular integrals in this paper is from the work of Doblare and Gracia<sup>[32]</sup>.

After the integration is computed, displacement BIE

provides linear algebraic equations like

$$u_{j,b} = f(d_1, \dots, d_i, \dots, d_N) \quad (25)$$

where  $d_i$  is an unknown degree of freedom.

When the docking point is near the edge of an element, the integration on the neighboring element becomes nearly singular and it is difficult to integrate accurately. Theoretically, we can use adaptive integration where the element to be integrated is subdivided or the line integral approach<sup>[34]</sup>, in which the integral is converted to line integrals. A simpler approach is employed in this research in order to increase the efficiency. In this approach, if the distance between the docking point and the edge of the element is less than a predetermined value, the shape function approach is used instead of using the displacement BIE (Fig. 3). The decision of the critical distance by which whether the shape function approach or BIE approach will be used is a trade-off between accuracy and efficiency.

## 5.2 The second method

The main idea of the second approach is shown in Fig. 4. In this approach, displacement BIE is used for the center point of each element, i.e., at  $(\xi, \eta) = (0, 0)$ , and the result is saved as

$$u_j^0 = f^0(d_1, \dots, d_i, \dots, d_N) \quad (26)$$

When the docking point on the element is determined, the equation for the displacement or traction is formulated using a new set of shape functions employing the value at the center point. The new shape functions are different from the element shape functions. They are used to generate constraint equations by algebraic operation and will not add computational overhead. Depending on the original shape functions used for integrating the BIE, the new shape functions to use will be decided.

### 5.2.1 For linear elements

The shape functions for linear triangular elements can be used for this case, in which the original element is divided into triangular cells with the center point being one of the vertices. Then, for the docking point  $b$ , a new equation is formed as:

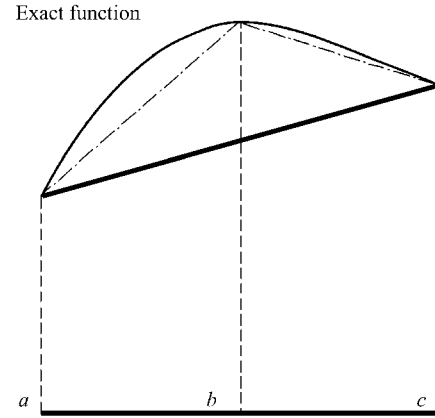


**Fig. 4** Concept of the second algorithm: the new approximation (dashdotted line) is more accurate than the original approximation (bold solid line) because of the additional point  $b$ .

$$u_{j,b} = N'_1(u_j)_1 + N'_2(u_j)_2 + N'_3 u_j^0 = f'(d_1, \dots, d_i, \dots, d_N) \quad (27)$$

where  $N'_i$  are the triangular shape functions which can be found in the Appendix.

The new equation is added to the system matrix with needed manipulations such as coordinate transformation and imposing boundary conditions and contact constraints.

### 5.2.2 For 8-node quadratic elements

The same procedure is necessary to produce the equations for the docking point except that 9-node Lagrangian interpolation is used. We have

$$u_{j,b} = N'_1(u_j)_1 + N'_2(u_j)_2 + N'_3(u_j)_3 + N'_4(u_j)_4 + N'_5(u_j)_5 + N'_6(u_j)_6 + N'_7(u_j)_7 + N'_8(u_j)_8 + N'_9 u_j^0 = f'(d_1, \dots, d_i, \dots, d_N) \quad (28)$$

where the 9-node shape functions can be found in the Appendix.

## 5.3 Formation of the system matrix

Once all the necessary equations are obtained as described above, the next step is to form the system matrix. There are many ways to assemble the system matrix. Whatever partitioning is selected, the tracking of the locations of the columns should be recorded carefully. In this study, the system matrix is partitioned as

$$\begin{bmatrix} \mathbf{A}_{nc} & \mathbf{0} & \mathbf{A}_c^u & \mathbf{0} & \mathbf{A}_c^t & \mathbf{0} \\ \mathbf{0} & \mathbf{B}_{nc} & \mathbf{0} & \mathbf{B}_c^u & \mathbf{0} & \mathbf{B}_c^t \\ \mathbf{0} & \mathbf{C}_A^1 & \mathbf{C}_A^2 & \mathbf{C}_A^3 & \mathbf{0} & \mathbf{C}_A^4 \\ \mathbf{0} & \mathbf{0} & \mathbf{0} & \mathbf{0} & \mathbf{C}_B^1 & \mathbf{C}_B^2 \end{bmatrix} \begin{Bmatrix} \mathbf{d}_A^{nc} \\ \mathbf{d}_B^{nc} \\ \mathbf{d}_A^u \\ \mathbf{d}_B^u \\ \mathbf{d}_A^t \\ \mathbf{d}_B^t \end{Bmatrix} = \begin{Bmatrix} \mathbf{f}_1 \\ \mathbf{f}_2 \\ \mathbf{f}_3 \\ \mathbf{f}_4 \end{Bmatrix} \quad (29)$$

Subscripts A and B refer to bodies A and B. Subscripts and superscripts nc and c mean non-contact and contact regions. Subscripts and superscripts u and t show the relationship to displacement and traction. Submatrices  $\mathbf{A}$  and  $\mathbf{B}$  are formulated from bodies A and B, and  $\mathbf{C}$  is formulated from contact constraints.

Because only part of the system matrix changes as the load increases, static condensation or other schemes can be employed to save the time in inverting the whole system matrix for each iteration. In addition, iterative solvers, such as generalized minimal RESidual (GMRES) or conjugate gradient (CG)<sup>[35]</sup>, can be utilized more effectively for this system than solving a fully populated system because this system is in some way banded as shown in Eq. (29).

Though each of the two algorithms can be implemented with both bilinear and quadratic elements, the first algorithm is implemented with bilinear elements and the second algorithm is implemented with quadratic elements in this paper. The reason is that the second algorithm can utilize 9-node Lagrangian shape functions when 8-node serendipity elements are used for the discretizations. The effectiveness and efficiency of the developed BEM code (in C++) with the proposed algorithms for 3-D contact analysis will be demonstrated in the next section with two test problems.

## 6 Numerical Examples

To test the developed 3-D BEM schemes for contact mechanics analysis, two examples are studied. The example problems are two typical 3-D contact problems with frictional contact.

To investigate whether the solution for a contact problem is accurate enough or not is a straightforward task. Solving 3-D contact problems and validating the results are still difficult tasks. Analytical solutions for contact problems are often limited to simple cases. Proving the existence and uniqueness of the solution for a contact problem in the general setting is still not

available<sup>[36]</sup>. These two limitations make it difficult to verify numerical methods including FEM and BEM for contact problems.

Even though the mathematically rigorous verification is almost impossible and how the model for a specific problem behaves as parameters change is still not understood well, FEM has been utilized to solve the real world problems and has turned out to be very successful in most of the applications. In this context, the FEM solutions are used in this study for comparison because the proposed BEM algorithms are supposed to be equivalent to the FEM regarding the accuracy, if not better. The developed BEM code has been verified using several stress analysis (non contact) problems before it is applied to solve the contact problems. In this study, the entire bodies in contact are meshed in both FEM (ANSYS) and BEM cases. The mesh for the BEM model is the same as the surface nodes and elements in the corresponding FEM mesh. The results of the BEM incorporating the proposed algorithms are compared with the ANSYS FEM results, although one to one comparison has limitations because many parameters, like values of the chosen penalty parameter (ANSYS only), are different and thus affect the FEM and BEM results.

### 6.1 Flat punch problem

This is a problem with conforming contact geometry, which is used first to test the developed BEM algorithm. The geometry and mesh of this example are shown in Fig. 5. The length, height, and width of the upper block are 1 m. The length, height, and width of the lower block are 2 m. Though the geometry is conforming, nonconforming mesh is used as shown in Fig. 5. For testing purposes, the material properties used for this test case are: Young modulus  $E = 1.0$  Pa and Poisson ratio  $\nu = 0.3$  for both contact bodies. Pressure of 0.1 Pa is applied for the upper surface of the punch (the upper block) and the lower surface of the foundation (the lower block) is constrained in all directions. Friction coefficient used in this example is 0.2.

For the FEM models, 4700 8-node linear elements and 1062 20-node quadratic elements are used. The contact parameters (normal stiffness, tangential stiffness, pinball radius, etc.) and iteration related parameters (total number of iteration, etc.) assigned by ANSYS version 5.7 as default are used for the FEM

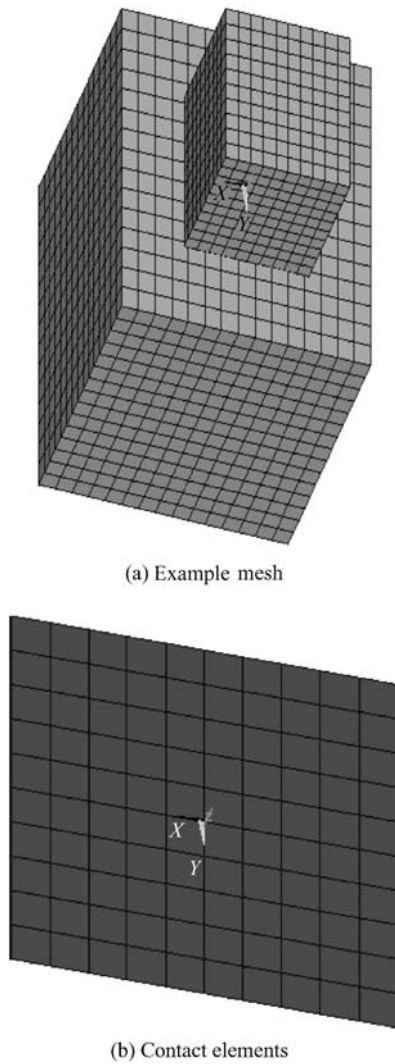


**Fig. 5 Geometry and mesh for flat punch problem**

models. For the BEM models, 1950 4-node linear elements and 702 8-node quadratic elements are used.

The analytical solution for a rigid punch on an infinite foundation has infinite stress values at the edges, which will not occur for elastic punch problem. This singularity in stress can cause numerical instability if the punch is much harder than the foundation.

The results for the normal displacement and normal pressure on the master surface along the positive  $X$ -axis (from the center of the lower surface of the upper block to the edge of the lower surface) are summarized in Figs. 6 and 7. Note that the BEM results in all the cases are comparable with the FEM results in showing the correct trend. However, both the FEM and BEM results exhibit some oscillations. The convergence from using linear elements to quadratic elements is not evident for both FEM and BEM. These discrepancies

may be due to the numerical difficulties in the nonlinear analysis and the (near) singular behaviors of the solution for this problem. Comparing with the published results in the literature, although the numerical values are not the same, because of the differences in geometries, material properties, and boundary conditions, the overall shapes of these plots (Figs. 6 and 7) show the similar trends as in the results published in Ref. [23]. Further study on selecting the parameters and using finer meshes can be conducted.

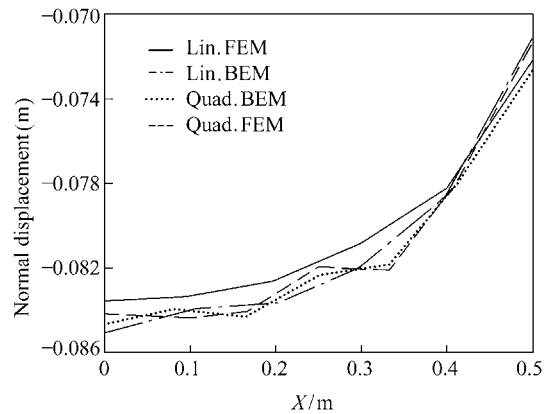


**Fig. 6 Displacement in the direction normal to contact surface and along the  $X$ -axis (block on block)**

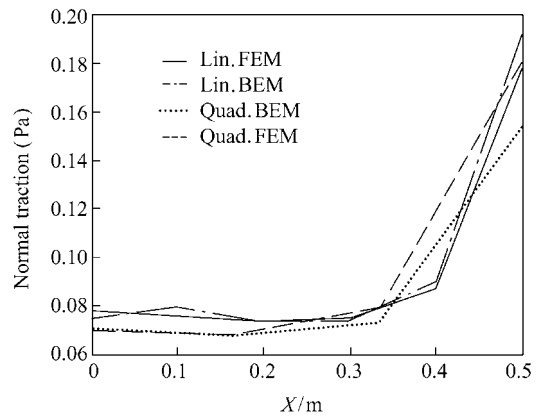


**Fig. 7 Normal traction on contact surface (block on block)**

### 6.2 Cylinder on block problem

This example is one of the nonconforming contact problems. The geometry and mesh for this example are shown in Fig. 8. The radius of the partial cylinder is 1.0 m, and the length along the axial direction is 1.0 m. The maximum height ( $Y$ -direction) of the partial cylinder is 0.5 m. The block has the dimensions of 1.0 m, 0.5 m, and 1.0 m in the  $X$ ,  $Y$ , and  $Z$  directions,

respectively. The material properties used are the same as those used for the previous example. For testing, a pressure of 0.01 Pa is applied to the upper surface of the partial cylinder and the lower surface of foundation (lower block) is constrained in all directions. The friction coefficient used in this example is also 0.2.

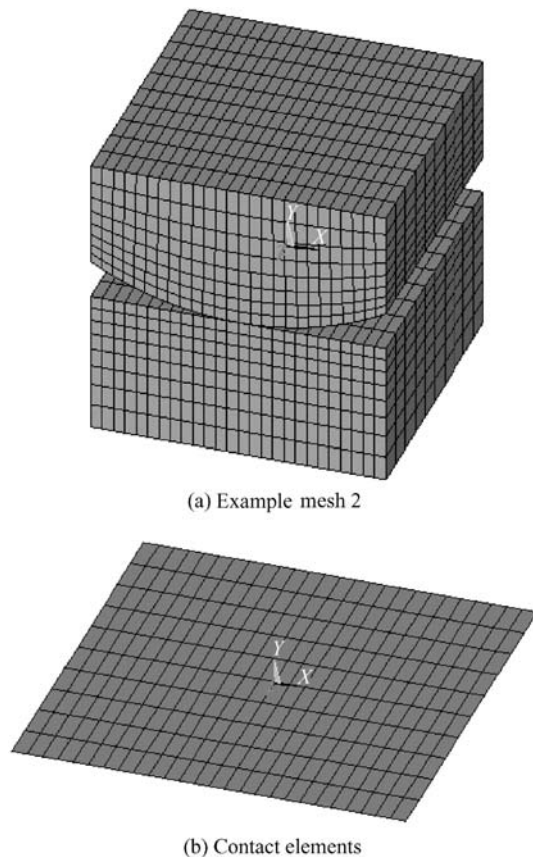


Fig. 8 Geometry and mesh of the second example

For the FEM models, 4160 8-node linear elements (coarse FEM) and 60 000 8-node linear elements (fine FEM) are used. The contact parameters (normal stiffness, tangential stiffness, pinball radius, etc.) and iteration related parameters (total number of iteration, etc.) assigned by ANSYS version 5.7 as default values are used for the FEM models. For the BEM models, 2192 4-node linear elements and 2192 8-node quadratic elements are used.

The results are summarized in Figs. 9 and 10. The  $X$  axis for the graphs starts from the center of the contact region and points in the direction shown in Fig. 8. In Fig. 9, the normal displacement result is plotted which shows good agreement regardless of the mesh density and the method used. The results for the normal contact pressure are compared with the Hertz result in Fig.

10 and show good agreement (Results are normalized by the Hertz' solution with the half width of the contact area  $a = 0.14$  m and the maximum contact pressure  $p_0 = 0.0455$  Pa), even though the Hertz solution is based on an infinitely long rigid cylinder in contact with an elastic half space<sup>[24]</sup>. When we consider the rigid cylinder assumption in the Hertz solution, the contact area may be larger for an elastic cylinder on an elastic foundation as shown in Fig. 10 because the elastic cylinder becomes flattened as the load increases. Note that the normal contact pressure changes in the  $Z$ -direction for any fixed  $X$  coordinate. For the Hertz's solution, this phenomenon does not happen because the Hertz solution is for a plane strain half space case.

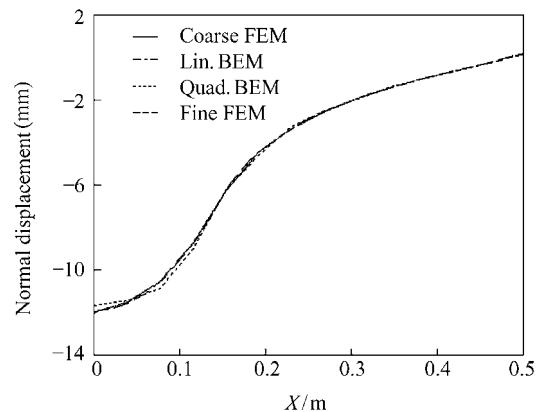


Fig. 9 Displacement in the direction normal to contact surface (cylinder on block)

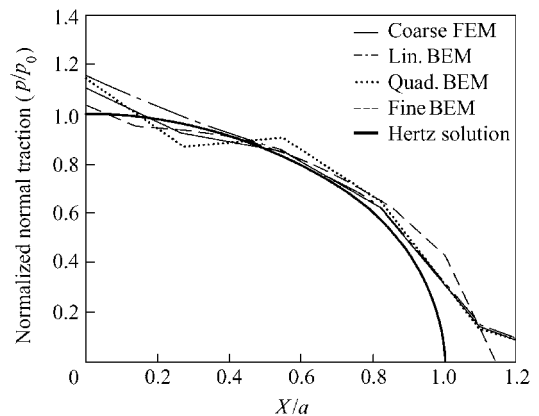


Fig. 10 Normal traction on contact surface (cylinder on block)

The results of the proposed BEM algorithms for the examples studied show a reasonable match with the FEM results (with about 5%–16% differences). The efficiency of the BEM in the solution, however, was not good for the given meshes. Considering that the

current implementation has a lot of room for improvement and that smaller numbers of BEM elements may have been sufficient to obtain results with similar accuracy, the efficiency difference may not be that large for real problems. In addition, total analysis time which includes preprocessing for building geometry and meshing can be much shorter with the BEM as compared with the FEM.

The loads applied for the example problems are compression only. The reason why the tangential load is not applied is that the possibility of rigid-body motion exists. Because current implementation is for solving static problems only, inertia force that can resist the rigid-body motion is not incorporated in the program. In other words, because at initial increments the load is so small that the contact force may not be large enough to hold the body without displacement constraints, or numerically, an initial gap may exist and the system matrix becomes singular or nearly singular. To avoid this problem, initial penetration can be imposed or temporary damping elements can be used. However, the algorithms proposed in this research can play an essential role as a foundation for solving dynamic contact problems, friction induced vibration problems, and large deformation problems.

## 7 Conclusions

Two algorithms for solving 3-D frictional contact problems by the BEM with nonconforming discretizations are proposed and implemented. To the authors' best knowledge, there is no published work dealing with the point-on-surface approach for 3-D contact problems. The BEM reported in this paper is only a preliminary step towards solving 3-D realistic contact problems. The developed BEM code for elastostatic cases can also be extended to solve contact problems with material and geometric nonlinearities and dynamic problems.

### Acknowledgement

The financial support to the first author (B. K.) by the University of Cincinnati is gratefully acknowledged.

### References

- [1] Anderson T, Allan-Persson B G. The boundary element method applied to two-dimensional contact problems with friction. In: Brebbia C A, ed. *Third International Seminar on Recent Advances in Boundary Element Methods*. Irvine: Springer, 1981.
- [2] Dandekar B W, Conant R J. Numerical analysis of elastic contact problems using the boundary integral equation method. Part 1: Theory. *International Journal for Numerical Methods in Engineering*, 1992, **33**: 1513-1522.
- [3] Hack R S, Becker A A. A general boundary element method approach to the solution of three-dimensional frictionless contact problems. *International Journal of Mechanical Sciences*, 1999, **41**: 419-436.
- [4] Huesman A, Kuhn G. Automatic load incrementation technique for plane elastoplastic frictional contact problems using boundary element method. *Computers & Structures*, 1995, **56**: 733-744.
- [5] Karami G. Boundary element analysis of two-dimensional elastoplastic contact problems. *International Journal for Numerical Methods in Engineering*, 1993, **36**: 221-235.
- [6] Olukoko O A, Becker A A. A new boundary element approach for contact problems with friction. *International Journal for Numerical Methods in Engineering*, 1993, **36**: 2625-2642.
- [7] Segond D, Tafreshi A. Stress analysis of three-dimensional contact problems using the boundary element method. *Engineering Analysis with Boundary Elements*, 1998, **22**: 199-214.
- [8] Takahashi S, Brebbia C A. A boundary element flexibility approach for solving contact problems with friction. *Engineering Analysis with Boundary Elements*, 1992, **4**: 24-30.
- [9] Landenberger A, El-Zafrany A. Boundary element analysis of elastic contact problems using gap finite elements. *Computers & Structures*, 1999, **71**: 651-661.
- [10] Yamazaki K, Sakamoto J, Takumi S. Penalty method for three-dimensional elastic contact problems by boundary element method. *Computers & Structures*, 1994, **52**: 895-903.
- [11] Kosior F, Guyot N, Maurice G. Analysis of frictional contact problem using boundary element method and domain decomposition method. *International Journal for Numerical Methods in Engineering*, 1999, **46**: 65-82.
- [12] Guyot N, Kosior F, Maurice G. Coupling of finite elements and boundary elements methods for study of the frictional contact problem. *Computer Methods in Applied Mechanics and Engineering*, 2000, **181**: 147-159.
- [13] Man K W. *Contact Mechanics Using Boundary Elements*. Southampton (UK): Computational Mechanics Publications, 1994.
- [14] Blazquez A, Paris F, Canas J, Garrido J A. An algorithm

- for frictionless contact problems with non-conforming discretizations using BEM. In: Brebbia C A, Dominguez J, Paris F, eds. *Boundary Element XIV*. Southampton: Computational Mechanics Publications, 1992: 409-420.
- [15] Paris F, Blazquez A, Canas J. Contact problems with non-conforming discretizations using boundary element method. *Computers & Structures*, 1995, **57**: 829-839.
- [16] Blazquez A, Paris F, Canas J. Interpretation of the problems found in applying contact conditions in node-to-point schemes with boundary element non-conforming discretizations. *Engineering Analysis with Boundary Elements*, 1998, **21**: 361-375.
- [17] Blazquez A, Paris F, Mantic V. BEM solution of two-dimensional contact problems by weak application of contact conditions with non-conforming discretizations. *International Journal of Solids and Structures*, 1998, **35**: 3259-3278.
- [18] Chen W H, Chen T C. Boundary element analysis for contact problems with friction. *Computers & Structures*, 1992, **45**: 431-438.
- [19] Martin D, Aliabadi M. A BE hyper-singular formulation for contact problems using non-conforming discretization. *Computers & Structures*, 1998, **69**: 557-565.
- [20] Iban A L, Garrido J A, Prieto I. Contact algorithm for non-linear elastic problems with large displacements and friction using the boundary element method. *Computer Methods in Applied Mechanics and Engineering*, 1999, **178**: 51-67.
- [21] Garrido J A, Forces A, Paris F. An incremental procedure for three-dimensional contact problems with friction. *Computers & Structures*, 1994, **50**: 201-215.
- [22] Ghaderi-Panah A, Fenner R T. A general boundary element method approach to the solution of three-dimensional frictionless contact problems. *Engineering Analysis with Boundary Elements*, 1998, **21**: 305-316.
- [23] Leahy J G, Becker A A. The numerical treatment of local variables in three-dimensional frictional contact problems using the boundary element method. *Computers & Structures*, 1999, **71**: 383-395.
- [24] Williams J A. *Engineering Tribology*. Oxford: Oxford University Press, 1994.
- [25] Johnson K L. *Contact Mechanics*. Cambridge: Cambridge University Press, 1985.
- [26] Gladwell G M L. *Contact Problems in the Theory of Elasticity*. The Netherlands: Sijthoff and Noordhoff, 1980.
- [27] Becker A A. *The Boundary Element Method in Engineering: A Complete Course*. McGraw Hill, 1992.
- [28] Beer G. *Programming the Boundary Element Method: An Introduction for Engineers*. New York: John Wiley & Sons, 2001.
- [29] Gao X, Davies T G. *Boundary Element Programming in Mechanics*. Cambridge: Cambridge University Press, 2002.
- [30] Brebbia C A, Dominguez J. *Boundary Elements—An Introductory Course*. New York: McGraw-Hill, 1989.
- [31] Dominguez-Hernandez J, Gracia L, Doblare M. A non-linear transformation algorithm for the integration of the singular kernels in 3D BEM for elastostatics. *Engineering Analysis with Boundary Elements*, 1995, **17**: 27-32.
- [32] Doblare M, Gracia L. On non-linear transformations for the integration of weakly-singular and cauchy principal value integrals. *International Journal for Numerical Methods in Engineering*, 1997, **40**: 3325-3358.
- [33] Guiggiani M, Gigante A. A general algorithm for multidimensional cauchy principal value integrals in the boundary element method. *Journal of Applied Mechanics*, 1990, **57**: 906-915.
- [34] Liu Y J. Analysis of shell-like structures by the boundary element method based on 3-D elasticity: Formulation and verification. *International Journal for Numerical Methods in Engineering*, 1998, **41**: 541-558.
- [35] Saad Y. *Iterative Methods for Sparse Linear Systems*. Boston: PWS Publishing, 1996.
- [36] Wriggers P. *Computational Contact Mechanics*. New York: John Wiley & Sons, 2002.

## Appendix: Lists of Shape Functions

The shape functions for 3-, 4-, 8-, and 9-node elements to interpolate two-dimensional functions on a surface are listed below for references.

For 3-node triangular element, the natural coordinates used are area coordinates. The shape functions for a 3-node linear triangular element are:

$$\begin{aligned} N_1 &= \xi, \\ N_2 &= \eta, \\ N_3 &= 1 - \xi - \eta. \end{aligned}$$

The natural nodal coordinates for 4-node bilinear elements are  $(-1, -1)$ ,  $(1, -1)$ ,  $(1, 1)$ , and  $(-1, 1)$  for node 1, 2, 3, and 4, respectively. The shape functions for 4-node bilinear elements are:

$$\begin{aligned} N_1 &= \frac{1}{4}(1 - \xi)(1 - \eta), \\ N_2 &= \frac{1}{4}(1 + \xi)(1 - \eta), \end{aligned}$$

$$N_3 = \frac{1}{4}(1 + \xi)(1 + \eta),$$

$$N_4 = \frac{1}{4}(1 - \xi)(1 + \eta).$$

The natural nodal coordinates for 8-node quadratic serendipity elements are  $(-1, -1)$ ,  $(1, -1)$ ,  $(1, 1)$ ,  $(-1, 1)$ ,  $(0, -1)$ ,  $(1, 0)$ ,  $(0, 1)$ , and  $(-1, 0)$  for node 1, 2, 3, 4, 5, 6, 7, and 8, respectively. The shape functions for 8-node serendipity elements are:

$$N_1 = \frac{1}{4}(1 - \xi)(1 - \eta)(-1 - \xi - \eta),$$

$$N_2 = \frac{1}{4}(1 + \xi)(1 - \eta)(-1 + \xi - \eta),$$

$$N_3 = \frac{1}{4}(1 + \xi)(1 + \eta)(-1 + \xi + \eta),$$

$$N_4 = \frac{1}{4}(1 - \xi)(1 + \eta)(-1 - \xi + \eta),$$

$$N_5 = \frac{1}{2}(1 - \xi^2)(1 - \eta),$$

$$N_6 = \frac{1}{2}(1 + \xi)(1 - \eta^2),$$

$$N_7 = \frac{1}{2}(1 - \xi^2)(1 + \eta),$$

$$N_8 = \frac{1}{2}(1 - \xi)(1 - \eta^2).$$

The shape functions for 9-node Lagrange elements are known as better shape functions for interpolating more complex functions than 8-node serendipity shape functions. The natural nodal coordinates for 9-node quadratic Lagrange elements are  $(-1, -1)$ ,  $(1, -1)$ ,  $(1, 1)$ ,  $(-1, 1)$ ,  $(0, -1)$ ,  $(1, 0)$ ,  $(0, 1)$ ,  $(-1, 0)$ , and  $(0, 0)$  for node 1, 2, 3, 4, 5, 6, 7, 8, and 9, respectively. The ninth shape function is called a bubble function due to its shape. The shape functions for a 9-node Lagrange element are:

$$N_1 = \frac{1}{4}\xi\eta(1 - \xi)(1 - \eta),$$

$$N_2 = -\frac{1}{4}\xi\eta(1 + \xi)(1 - \eta),$$

$$N_3 = \frac{1}{4}\xi\eta(1 + \xi)(1 + \eta),$$

$$N_4 = -\frac{1}{4}\xi\eta(1 - \xi)(1 + \eta),$$

$$N_5 = -\frac{1}{2}\eta(1 - \xi^2)(1 - \eta),$$

$$N_6 = \frac{1}{2}\xi(1 + \xi)(1 - \eta^2),$$

$$N_7 = \frac{1}{2}\eta(1 - \xi^2)(1 + \eta),$$

$$N_8 = -\frac{1}{2}\xi(1 - \xi)(1 - \eta^2),$$

$$N_9 = (1 - \xi^2)(1 - \eta^2).$$